

An enhanced high-resolution EMCCD-based gamma camera using SiPM side detection

This article has been downloaded from IOPscience. Please scroll down to see the full text article.

2010 Phys. Med. Biol. 55 6773

(<http://iopscience.iop.org/0031-9155/55/22/011>)

View [the table of contents for this issue](#), or go to the [journal homepage](#) for more

Download details:

IP Address: 131.180.130.114

The article was downloaded on 21/12/2010 at 12:29

Please note that [terms and conditions apply](#).

An enhanced high-resolution EMCCD-based gamma camera using SiPM side detection

J W T Heemskerk^{1,2}, M A N Korevaar^{1,2}, J Huizenga², R Kreuger²,
D R Schaart², M C Goorden^{1,2} and F J Beekman^{1,2,3}

¹ Department of Nuclear Medicine, Image Sciences Institute, University Medical Center Utrecht, Room STR 5.153, Universiteitsweg 100, 3584 CG, Utrecht, The Netherlands

² Section Radiation Detection and Medical Imaging, Department Radiation, Radionuclides, Reactors, Delft University of Technology, Mekelweg 15, 2629 JB Delft, The Netherlands

³ MILabs Molecular Imaging Laboratories, Universiteitsweg 100, STR 5.203, 3584 CX Utrecht, The Netherlands

E-mail: freek@isi.uu.nl

Received 3 May 2010, in final form 13 September 2010

Published 28 October 2010

Online at stacks.iop.org/PMB/55/6773

Abstract

Electron-multiplying charge-coupled devices (EMCCDs) coupled to scintillation crystals can be used for high-resolution imaging of gamma rays in scintillation counting mode. However, the detection of false events as a result of EMCCD noise deteriorates the spatial and energy resolution of these gamma cameras and creates a detrimental background in the reconstructed image. In order to improve the performance of an EMCCD-based gamma camera with a monolithic scintillation crystal, arrays of silicon photon-multipliers (SiPMs) can be mounted on the sides of the crystal to detect escaping scintillation photons, which are otherwise neglected. This will provide *a priori* knowledge about the correct number and energies of gamma interactions that are to be detected in each CCD frame. This information can be used as an additional detection criterion, e.g. for the rejection of otherwise falsely detected events. The method was tested using a gamma camera based on a back-illuminated EMCCD, coupled to a 3 mm thick continuous CsI:Tl crystal. Twelve SiPMs have been mounted on the sides of the CsI:Tl crystal. When the information of the SiPMs is used to select scintillation events in the EMCCD image, the background level for ^{99m}Tc is reduced by a factor of 2. Furthermore, the SiPMs enable detection of ¹²⁵I scintillations. A hybrid SiPM-/EMCCD-based gamma camera thus offers great potential for applications such as *in vivo* imaging of gamma emitters.

1. Introduction

Single-photon emission computed tomography (SPECT) is a prominent molecular imaging modality, both in clinical and in pre-clinical (e.g. small-animal) research. The application of pinhole geometries leads to unsurpassed imaging capabilities in small-animal SPECT (Schramm *et al* 2003, Beekman *et al* 2005, Van der Have *et al* 2009) and is also applied for human SPECT imaging of specific regions-of-interest, e.g. brain, chest and extremities (Rowe *et al* 1993, Funk *et al* 2006, Ostendorf *et al* 2006, respectively). For introductions to pinhole and small-animal SPECT imaging see e.g. King *et al* (2002), Meikle *et al* (2005) and Beekman and Van der Have (2007).

Gamma detectors with high intrinsic spatial resolutions in combination with energy discrimination capabilities may be essential for the improvement of future multi-pinhole SPECT devices, as has been shown by simulations and modeling in (e.g.) Rogulski *et al* (1993), Beekman and Vastenhout (2004), Meng *et al* (2006), Rentmeester *et al* (2007), Shokouhi *et al* (2009) and Goorden *et al* (2009); recent work by Meng *et al* (2009a) validates the efficacy of high-resolution detectors in small-animal SPECT applications. High-resolution gamma-ray detectors have been developed for applications ranging from astronomy and particle physics to biomedical imaging. These detectors have either been based on direct detection of gamma rays in semiconductor material (e.g. Matteson *et al* (1997), Barber (1999), He *et al* (1999), Wagenaar *et al* (2003), Kataoka *et al* (2005), Ponchut *et al* (2005), Accorsi *et al* (2008), Meng *et al* (2009b), Peterson *et al* (2009) and Russo *et al* (2009)), scintillation detection employing high-resolution position-sensitive light sensors (e.g. Menard *et al* (1998), Fiorini *et al* (2003), Lees *et al* (2003), Beekman and De Vree (2005), Nagarkar *et al* (2006), Miller *et al* (2006), Soesbe *et al* (2007) and Meng and Fu (2008)) or even a combination of both (Miyata *et al* 2004).

For scintillation detectors, very high spatial accuracy (below 60 μm) can be obtained with a detector consisting of an EMCCD operating at high frame rates that detects individual gamma photons in an optically coupled micro-columnar CsI:Tl scintillation crystal with the use of scintillation detection algorithms (e.g. De Vree *et al* (2005), Miller *et al* (2006), Nagarkar *et al* (2006), Heemskerk *et al* (2007), Meng and Fu (2008), Westra *et al* (2009)). To improve the applicability for medical imaging, the application of continuous (or monolithic) crystals can improve the sensitivity for incoming $^{99\text{m}}\text{Tc}$ gamma photons (140 keV) at some cost in spatial and energy resolution (Korevaar *et al* 2009a, Heemskerk 2010).

The spatial and energy resolution obtained with continuous crystals is, in principle, reduced because of the increased width of the light spread distribution compared to micro-columnar crystals. This can partly be overcome by the use of detection algorithms that take into account the depth-dependent light spread distribution (Korevaar *et al* 2009a)⁴. With such a depth-sensitive algorithm, EMCCD-based gamma cameras equipped with monolithic, 2.6 mm thick CsI:Tl crystals (corresponding to 60% $^{99\text{m}}\text{Tc}$ absorption) have achieved a spatial resolution of $\sim 150 \mu\text{m}$, (intrinsic) depth-of-interaction correction and an energy resolution of 48% for $^{99\text{m}}\text{Tc}$ imaging (Korevaar *et al* 2009a, 2009b); the application of micro-retroreflectors even improves the energy resolution to 34% (Heemskerk *et al* 2009).

However, noise in the EMCCD complicates the detection of scintillation events occurring at some distance from the EMCCD surface (i.e. in the top of the scintillation crystal). In particular, the detection of $\sim 30 \text{ keV}$ ^{125}I gamma photons (and characteristic x-rays) is significantly compromised, as these photons are absorbed at a greater distance from the detector surface (over 50% of ^{125}I gamma photons are absorbed in the top 200 μm of the

⁴ The multi-scale algorithm actually uses information from the light spread to deduce the depth at which the scintillation occurred (the depth of interaction or DOI).

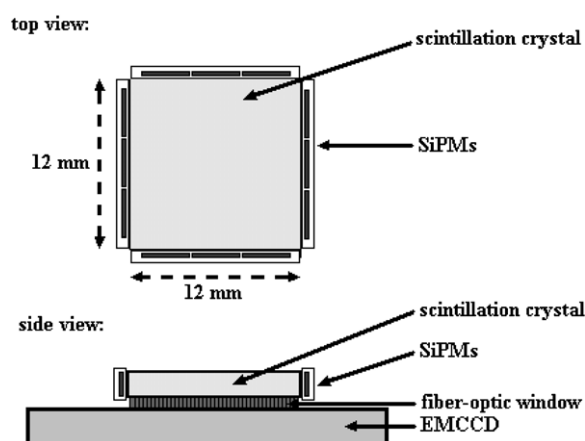


Figure 1. Experimental EMCCD-based gamma camera set-up with SiPM side detectors. A Peltier element cools the EMCCD chip to reduce its dark current. Silicon photon-multipliers (SiPMs) are coupled to the sides of the scintillation crystal. The crystal and SiPMs are also cooled through thermal contact with the EMCCD.

CsI:Tl crystal) and generate far less scintillation photons than $^{99\text{m}}\text{Tc}$ (approx. 25%). As a result, true scintillation events can hardly be distinguished from the background, which may lead to a background of falsely detected events in the reconstructed image or loss of sensitivity when thresholding is applied. Additional information on the true number of scintillation events therefore could assist the detection algorithm in separating true- from false-positive detections.

Since most light detectors (including EMCCDs) read out only a single surface of the scintillation crystal, a considerable amount of scintillation photons is lost because they escape from the sides (see e.g. Gruner *et al* (2002)); taking into account internal reflections within the crystal this could amount to 40–60% of the total number of scintillation photons. The information that these photons contain about the position and energy of the scintillation events has thus far not been exploited in CCD-based gamma imaging.

In this paper, we introduce a novel method (Beekman 2007) to use the information from these photons; silicon photomultipliers (SiPMs, Bondarenko *et al* 2000, Buzhan *et al* 2003, Yamamoto *et al* 2007) attached to the sides of the crystal (see figure 1) are used to detect the previously neglected photons. The information that is extracted from the SiPM signals consists of the number of scintillation events in each measured frame; this number will serve as *a priori* information for the detection algorithm. To investigate the efficacy of our hybrid SiPM-enhanced EMCCD-based gamma camera, we compare its performance in terms of signal-to-background ratio (SBR), spatial and energy resolution for $^{99\text{m}}\text{Tc}$ and ^{125}I imaging to the same setup without SiPMs.

2. Materials and methods

2.1. EMCCD gamma camera

The scintillation gamma camera that is used in this research consists of a scintillation crystal coupled to an EMCCD and is operated in gamma photon-counting mode, see figure 1. Gamma photons are converted in the crystal and the individual scintillation flashes are detected by the

EMCCD. A comprehensive description of this gamma camera is provided elsewhere (de Vree *et al* 2005, Heemskerk *et al* 2007).

We use a 3 mm thick continuous CsI:Tl crystal, which is proximity-coupled to the EMCCD via a fiber-optic plate using optical grease. The crystal has an interaction probability of $\sim 66\%$ for 141 keV ^{99m}Tc gamma photons and $\sim 100\%$ for ~ 30 keV ^{125}I gamma photons and x-rays. The emission spectrum of the scintillation photons of the crystal has a maximum at 550 nm.

The EMCCD used here is a back-illuminated CCD97 from E2V technologies. The quantum efficiency of the CCD97 surpasses 90% in the range of visible light between 500 and 650 nm, which matches nicely with the spectral emission of the crystal. It has an active area of 512 lines of 512 pixels, each $16 \times 16 \mu\text{m}^2$ in size. To reduce the dark current to a level below $0.1 \text{ e}^- \text{ pixel}^{-1} \text{ s}^{-1}$, the EMCCD is cooled to a temperature of -50°C using a Peltier element backed by a liquid cooler. The readout of the EMCCD is performed by an in-house developed electronics board; by reading out the EMCCD lines in pairs of two, we achieve a frame rate of 50 Hz (De Vree *et al* 2004).

The frames are transferred to a Matrox Meteor-II framegrabber. The camera is operated in gamma photon-counting mode by off-line processing with an analytical scintillation detection algorithm (Korevaar *et al* 2009a). This algorithm analyzes each separate frame for the presence of (possibly multiple) scintillations and determines the spatial coordinates and the intensity of each individually detected event, presenting the data in list mode (indicating x , y , z -coordinates, intensity and frame number).

2.2. Silicon photo-multipliers

SiPMs are photon detectors that consist of a large number of avalanche photo-diodes (APDs) connected in parallel and operated in Geiger mode (Bondarenko *et al* 2000, Buzhan *et al* 2003). When a single APD (or: micro-cell) detects an optical photon, it will discharge, resulting in an output signal with fixed charge content. The presence of a large number of these APDs in a single SiPM basically presents a proportional photon counter, provided that the photon density is sufficiently low (i.e. when no more than a single photon is detected within the recovery time of the microcell, see, e.g., Van Dam *et al* (2010)). The accumulated signal of the cells in an SiPM is proportional to the number of cells discharging (i.e. increasing with the number of photons that is detected). SiPM readout of scintillator crystals currently enjoys increasing interest for medium energy gamma detectors, in particular for (time-of-flight) positron emission tomography (PET) (Kim *et al* 2008, Schaart *et al* 2009, 2010), combined PET-MRI (España *et al* 2008) and small-animal PET (Llosá *et al* 2008).

We have selected Hamamatsu S10931-100P(X)-type SiPMs, which are $3 \times 3 \text{ mm}^2$ in size and consist of $900 \times 100 \times 100 \mu\text{m}^2$ cells. On all four sides of the crystal, three SiPMs have been mounted using Bicon BC-630 optical grease. Through thermal contact with the EMCCD, the SiPMs are cooled to a temperature of $-27.4 (\pm 0.2)^\circ\text{C}$ and they are operated at a bias voltage of approx. 67.4 V. For each SiPM, the bias voltage can be adjusted separately, to ensure relatively equal gain and noise levels. The spectral response of the SiPMs peaks at 400 nm, which lies somewhat lower than the peak emission of the CsI:Tl crystal; nevertheless, the photon-detection efficiency should be around 20–25% (Yamamoto *et al* 2007).

In this first proof-of-principle setup, the SiPMs are applied as gamma photon counters. The signals of the 12 SiPMs are first preamplified by a 16-channel read out board (the design of which is described and characterized in Seifert *et al* (2008)) and subsequently summed. The summed signal is shaped and amplified by an Ortec 572 spectroscopy amplifier. Spectra of the amplitudes of the sum pulses are recorded by an Ortec AD114 peak-sensitive ADC and these spectra are used to set an appropriate threshold on a Canberra SCA 2035 constant fraction

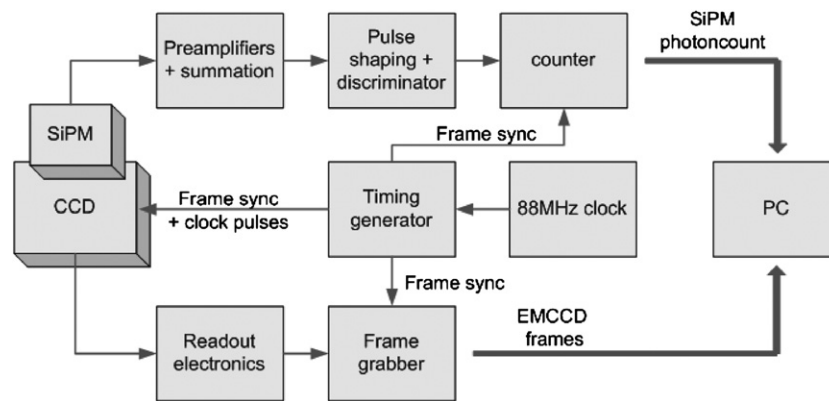


Figure 2. Simplified electronics scheme of the SiPM-enhanced EMCCD-based gamma camera. The gamma photon count of the SiPMs can be applied as *a priori* knowledge for the analytic scintillation detection algorithm. A timing circuit ensures synchronization between the EMCCD frames and the counter for the SiPM pulses.

discriminator (CFD). The CFD logic output pulses are counted with a National Instruments PCI-6034E card. A simplified electronics scheme for the SiPM-enhanced EMCCD-based gamma camera is shown in figure 2.

In order to synchronize the frames of the EMCCD with the pulse count of the SiPMs, the PCI-6034E card (which counts the SiPM pulses) also records the EMCCD's frame synchronization pulse. Furthermore, at the start of each data acquisition (of 2000 frames), a single pulse is sent in parallel to a LED and a third channel on the PCI-6034 card. A light flash appears in one of the first EMCCD frames in coincidence with a single pulse on the PCI-6034E card. These coincident start pulses are used to indicate which EMCCD frame corresponds to which interval on the counter.

2.3. Use of SiPM signals

To include almost all SiPM sum signals within the SiPM photopeak, the CFD threshold has been set at *photopeak position* – *FWHM* (of the SiPM pulse-height spectra) for both the ^{99m}Tc and the ^{125}I measurements. The number of events above the threshold is counted per EMCCD frame. The effect of the inclusion of this *a priori* SiPM information on the performance of the gamma camera is investigated for each source by either disregarding or including the SiPM count information in the post-processing scintillation detection algorithm.

Two methods for using the SiPM event count are compared, which will be denoted as the *rejection* and the *counting* method. In the *rejection* method, which is based on the notion that the number of incident gammas in a small-animal pinhole geometry is expected to be less than one per frame (Beekman and Vastenhouw 2004, Rentmeester *et al* 2007 and Van der Have *et al* 2009), those frames for which the SiPMs detect no events are simply discarded. In the more advanced *counting* method, the SiPM count is used to select the number of scintillation events that the scintillation detection algorithm detects in each frame.

In practice this means that for the *rejection* method, when the SiPMs indicate the presence of scintillation events (disregarding how many) in a certain EMCCD frame, *all* events detected by the EMCCD algorithm are included. For the *counting* method, the number of counts indicated by the SiPM is used explicitly in the analysis. In this case the corresponding number

of EMCCD events, in order of highest energy (as determined by the EMCCD), is selected. Therefore, the *rejection* method will include some counts (i.e. those detected by EMCCD, but not by the SiPMs) that will be excluded by the *counting* method. For both methods, should the EMCCD detect less counts than the SiPMs, some counts will be lost.

Both the *rejection* and the *counting* method are compared to the case where the SiPM information is ignored and *all* counts indicated by the EMCCD are included.

2.4. Measurements

In order to verify the performance of the SiPMs and to set the appropriate thresholds for the CFD, the hybrid gamma camera has been irradiated by both ^{99m}Tc and ^{125}I flood and line sources. The line sources are created by collimation using a 30 μm wide slit in 4 mm thick tungsten plates.

For measurements of the spatial and energy resolution of the hybrid gamma camera the crystal is irradiated by ^{99m}Tc and ^{125}I line sources only. Data were acquired for $\sim 25,000$ frames for each source. In order to determine the energy resolution for the camera without SiPMs, energy spectra are constructed as histograms of the intensities of the detected events, such as determined by the scintillation detection algorithm (Korevaar *et al* 2009a).

The energy spectra of the EMCCD are used to determine the energy windows for reconstruction of the image of the slit and determination of the spatial resolution. For a fair comparison of the efficacy of the SiPMs, for both the camera with and without SiPMs, the energy windows are set to range from 50% to 150% of the position of the full-energy peak of the EMCCD spectrum (cf Heemskerk *et al* (2009)). This is because in the current setup the SiPMs indicate how many events, detected by the scintillation detection algorithm, to be included in the listmode; the SiPMs' information does not influence the location or energy of detected events.

The spatial resolution is determined by measuring the full-width-at-half-maximum (FWHM) of the projection of the slit, corrected for the width of the slit itself by deconvolution (Beekman and De Vree 2005). For ^{99m}Tc , we have determined the uncertainty of the spatial resolution by using the jackknife method (Miller 1974). The SBR is defined as the *net* number of counts within the area irradiated by the slit (taken to be 50 lines for ^{99m}Tc and 200 lines for ^{125}I) divided by the number of false positives in an equally sized area of the EMCCD covered by the tungsten plate (i.e. a non-irradiated area). The number of net signal counts is obtained by correcting the total signal for the false positives (cf Korevaar *et al* (2009a), Heemskerk *et al* (2009)); the background is counted for the entire EMCCD and scaled to the irradiated area.

3. Results

3.1. Characterization of SiPMs

In figure 3, we show the ^{125}I and ^{99m}Tc pulse-height spectra of the SiPMs measured for both line and flood sources. The good agreement between the spectra of the line sources and those of the flood sources indicates that the overall summed signal of the SiPMs (i.e. the total number of detected scintillation photons) is relatively independent of the location of the scintillation events in the crystal. The difference in peak positions of the ^{99m}Tc and ^{125}I spectra indicates a decent separability of the SiPMs' response with the deposited gamma energy, in the range of energies investigated.

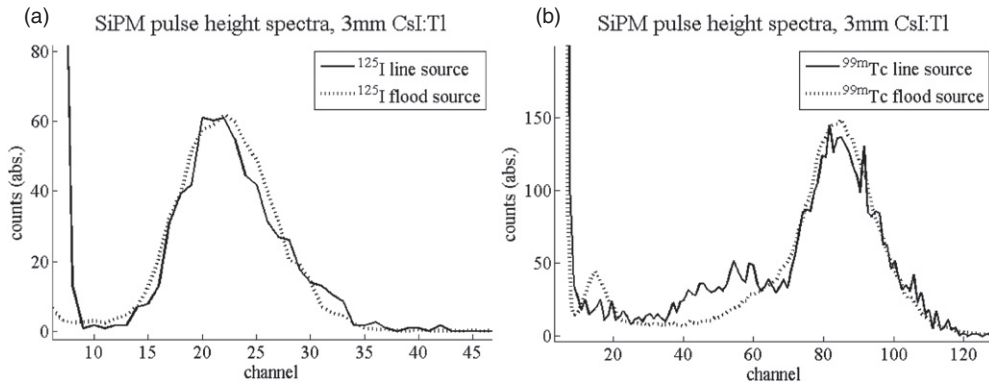


Figure 3. SiPM pulse-height spectra for ^{125}I (a) and $^{99\text{m}}\text{Tc}$ (b) sources. In both cases, the SiPM pulses can be clearly distinguished from the background. For the $^{99\text{m}}\text{Tc}$ line source (solid (b)), the spectrum seems to indicate a slight increase of scatter (to the left of the photopeak), presumably arising from the collimating slit.

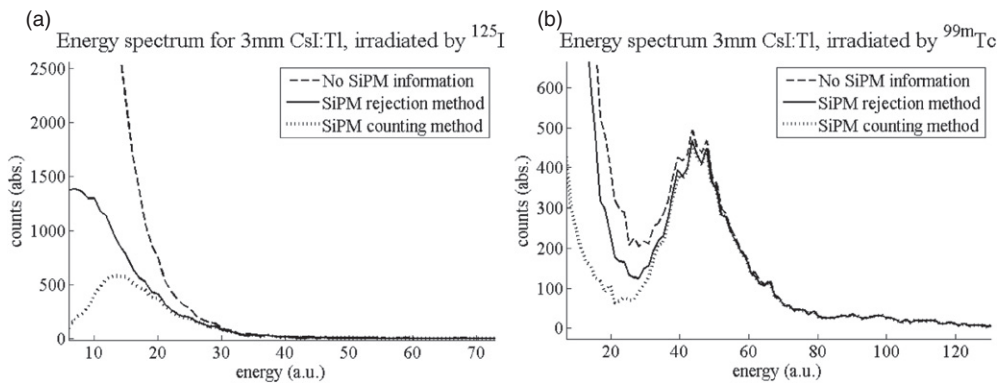


Figure 4. EMCCD energy spectra of the ^{125}I (a) and $^{99\text{m}}\text{Tc}$ (b) signal for the camera with the SiPMs' event count ignored (dashed curves), with the *rejection* method (solid curves) and the more advanced *counting* method (dotted curves).

3.2. EMCCD energy spectra

Figure 4 shows the energy spectra that have been acquired with the EMCCD. Values for the energy resolution are included in table 1. It is clear that by including the SiPM information the energy spectra are improved dramatically by the rejection of false-positive events. For $^{99\text{m}}\text{Tc}$, the background of low-energy counts (below the full-energy peak) is significantly suppressed. In the case of ^{125}I , it is not even possible to separate true positives from the background without applying the SiPMs. Compared to the *rejection* method, the *counting* method clearly leads to further reduction of the background level.

3.3. Spatial resolution and SBR

Figure 5 shows the profiles of the images of the line sources, from which we have measured the FWHM spatial resolution values, for the camera employing the *rejection* and *counting*

Table 1. Energy resolution (in FWHM (%)) measured from the EMCCD energy spectra (figure 4) and spatial resolution values (FWHM and FWTM (μm)) and signal-to-background ratio (SBR) as measured from the slit image profiles (figure 5). For ^{125}I the resolution has been determined after subtraction of a background level. The SBR is defined as the net number of counts within the image of the slit, divided by those in an equally sized area that is not irradiated.

	^{125}I			$^{99\text{m}}\text{Tc}$		
	SiPMs ignored	With SiPMs		SiPMs ignored	With SiPMs	
		<i>Rejection</i>	<i>Counting</i>		<i>Rejection</i>	<i>Counting</i>
EMCCD energy resolution FWHM	No photopeak	–	~ 30 keV ($\sim 100\%$)	75 ± 2 keV (54%)	68 ± 3 keV (48%)	69 ± 2 keV (49%)
Spatial resolution FWHM	~ 1900 μm	~ 1700 μm	~ 1600 μm	$164 (\pm 4)$ μm	$162 (\pm 4)$ μm	$160 (\pm 3)$ μm
Spatial resolution FWTM	–	–	–	$551 (\pm 16)$ μm	$524 (\pm 16)$ μm	$519 (\pm 23)$ μm
Signal/false-positive counts (SBR)	2092/18465 (0.11)	4029/4396 (0.92)	2585/1285 (2.0)	7071/205 (34.5)	6569/138 (47.5)	6493/100 (64.7)

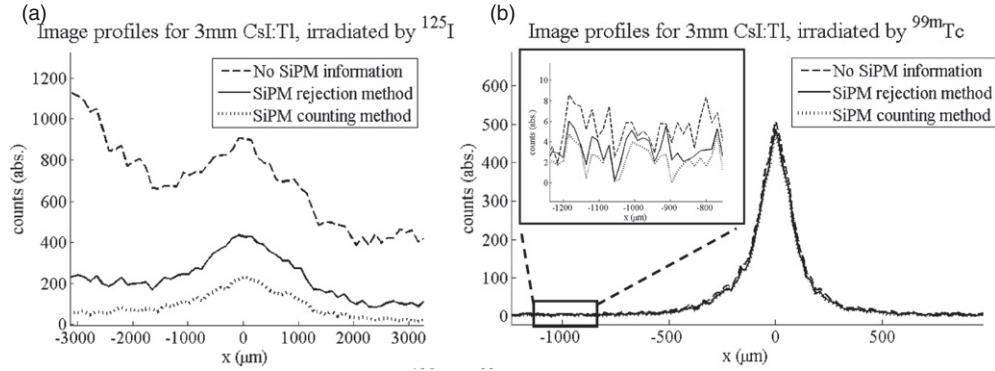


Figure 5. Profiles of the images of the ^{125}I (a) and $^{99\text{m}}\text{Tc}$ (b) line sources for the gamma camera for the *rejection* and *counting* methods and without the application of the SiPMs. The insert (for $^{99\text{m}}\text{Tc}$ (b)) zooms in on part of the profile to illustrate the reduction of the background.

methods and without including the information of the SiPMs. Spatial resolution and SBR derived from figure 5 are included in table 1.

For $^{99\text{m}}\text{Tc}$, one can see that the application of the SiPMs reduces the background without significantly reducing the signal itself. For ^{125}I , the improvement of the profile of the slit (i.e. the spatial resolution) and the reduction of the background are striking. In particular, the *counting* method allows the ^{125}I scintillations to be distinguished from the background, although significant blurring occurs due to the relatively low number of scintillation photons generated at ~ 30 keV. However, without the information from the SiPMs, applying only the energy window, it is only barely possible to distinguish any ^{125}I signal from the background.

For the ^{125}I measurements, the background across the detector is, unfortunately, not uniform. We believe this background is due either to noise in the EMCCD itself or to noise in the readout electronics. However, this lack of uniformity should not affect our conclusions

regarding the SBR because the SBR comparison includes the false positives for the entire area of the EMCCD and is furthermore performed on the same data set (i.e. EMCCD frames) for all methods.

4. Discussion

In the present investigation, we have shown that the use of *a priori* knowledge of the SiPMs can improve the performance of our EMCCD-based gamma camera. Two specific improvements can be noted: first, it is now possible to detect ^{125}I scintillations, which could barely be distinguished from the background before; the SBR for ^{125}I has improved by a factor of almost 20. Secondly, for $^{99\text{m}}\text{Tc}$, the SBR has been improved by a factor of almost 2.

From the profiles of the line sources, we can see that the rejection of frames without SiPM counts (i.e. most likely dark frames) already leads to reduction of the background level (false-positive counts), namely an improvement of 33% in the case of $^{99\text{m}}\text{Tc}$. Using the SiPM gamma photon count as an estimator of the number of most likely events from the scintillation detection algorithm leads to a further improvement (an additional 50%). Furthermore, the energy spectra show that applying the SiPMs' information also significantly reduces the number of false counts in the EMCCD images.

Even with the application of SiPMs, the spatial resolution for ^{125}I is lower than with micro-columnar crystals (Heemskerk *et al* 2007, Meng and Fu 2008). Due to the monolithic nature of the scintillator and its thickness, low-energy ^{125}I gammas and x-rays give rise to spotsizes of several mm^2 on the EMCCD. These are hard to localize the same spatial accuracy as is possible with columnar crystals. However, with the help of the SiPMs, these events can much better be distinguished from the background.

In this work, we have used the SiPMs only to indicate the number of scintillation events in each frame. In principle, more information can be extracted from the SiPMs, the use of which might further improve gamma camera performance. In particular, the energy resolution of the SiPMs for ^{125}I and $^{99\text{m}}\text{Tc}$ (53% and 29%, respectively) is significantly better than that of the EMCCD. In future work, we hope to use the signal of the SiPMs to further improve the energy resolution of the EMCCD-based gamma camera by combining pulse-height information from the SiPMs with the energy estimation from the scintillation detection algorithm. Other near-future investigations will include the extraction of spatial information from the pulse-heights of the individual SiPMs. This spatial information will allow us to exclude areas of the EMCCD from the scintillation detection algorithm for further improvements of the noise performance of our gamma camera as well an acceleration of the algorithm (Beekman 2007). Ultimately, for a very large area EMCCD, a high frame rate could be maintained by a partial read out, based on the information provided by the SiPM side detectors. Also, the SiPMs might improve the detection of (partially) overlapping scintillation flashes, which can cause problems with the analytical multi-scale algorithm used here. Finally, the method shown here could be combined with other methods such as micro-retroreflectors or optimized scintillation crystal materials (Heemskerk *et al* 2009, Heemskerk 2010) for further improvement of the energy resolution.

5. Conclusion

In this paper, we have combined the benefits of the good signal-to-noise ratio of SiPMs with the good spatial resolution of EMCCD-based gamma cameras. It has been shown that for $^{99\text{m}}\text{Tc}$, SiPM side detectors improve the gamma camera signal-to-background ratio, while the good detection efficiency and excellent spatial resolution are maintained. Moreover, the application

of SiPMs allows detection of ^{125}I scintillations with thick continuous scintillators necessary for higher energy photons, which could previously hardly be achieved. For future investigations, we hope to include energy and spatial information from the SiPMs in the detection algorithm to further improve the accuracy of this hybrid gamma camera.

We conclude that both SiPMs and EMCCD are suitable devices for scintillation gamma detection, and that a hybrid SiPM/EMCCD gamma camera can combine the advantages of both types of light sensor: high spatial resolution and excellent SBR. Thus, hybrid SiPM/EMCCD gamma cameras show promise for enhancing future SPECT and gamma autoradiography devices.

Acknowledgments

This work has been sponsored in part by the Netherlands Ministry of Economic Affairs, IOP photonics grant IPD067766. The authors would like to thank S Seifert for valuable discussions and technical assistance.

References

- Accorsi R, Celentano B, Laccetti P, Lanza R C, Marotta M, Mettievier G, Montesi M C, Roberti G and Russo P 2008 High-resolution ^{125}I small animal imaging with a coded aperture and a hybrid pixel detector *IEEE Trans. Nucl. Sci.* **55** 481–90
- Barber H B 1999 Applications of semiconductor detectors to nuclear medicine *Nucl. Instrum. Methods A* **436** 102–10
- Beekman F 2007 Radiation detection device, scintillation device and detection method, as well as multiple image-forming device *Patent Application* No WO/2007/043868
- Beekman F J and De Vree G A 2005 Photon-counting versus an integrating CCD-based gamma camera: important consequences for spatial resolution *Phys. Med. Biol.* **50** N109–19
- Beekman F J and Van Der Have F 2007 The pinhole: gateway to ultra-high-resolution three-dimensional radionuclide imaging *Eur. J. Nucl. Med. Mol. Imaging* **34** 151–61
- Beekman F J and Vastenhout B 2004 Design and simulation of a high-resolution stationary SPECT system for small animals *Phys. Med. Biol.* **49** 4579–92
- Beekman F J, Van Der Have F, Vastenhout B, Van Der Linden A J A, Van Rijk P P, Burbach J P H and Smidt M P 2005 U-SPECT-I: a novel system for sub-millimeter resolution tomography of radiolabeled molecules in mice *J. Nucl. Med.* **46** 1194–200
- Bondarenko G *et al* 2000 Limited Geiger-mode microcell silicon photodiode: new results *Nucl. Instrum. Methods A* **442** 187–92
- Buzhan P *et al* 2003 Silicon photomultiplier and its possible applications *Nucl. Instrum. Methods A* **504** 48–52
- De Vree G A, Westra A H, Moody I, Van Der Have F, Ligtoet C M and Beekman F J 2004 Electronics for a photon-counting gamma camera based on an electron-multiplying CCD *IEEE Nucl. Sci. Symp. Conf. Record 2004* pp 4159–63
- De Vree G A, Westra A H, Moody I, Van Der Have F, Ligtoet C M and Beekman F J 2005 Photon-counting gamma camera based on an electron-multiplying CCD *IEEE Trans. Nucl. Sci.* **52** (Part 1) 580–8
- España S, Tapias G, Fraile L M, Herraiz J L, Vicente E, Udias J, Desco M and Vaquero J J 2008 Performance evaluation of SiPM detectors for PET imaging in the presence of magnetic fields *IEEE Nucl. Sci. Symp. Conf. Record 2008* pp 3591–5
- Fiorini C, Longoni A, Perotti F, Labanti C, Rossi E, Lechner P, Soltau H and Struder L 2003 A monolithic array of silicon drift detectors coupled to a single scintillator for gamma-ray imaging with sub-millimeter position resolution *Nucl. Instrum. Methods A* **512** 265–71
- Funk T, Kirch D L, Koss J E, Botvinick E and Hasegawa B H 2006 A novel approach to multipinhole SPECT for myocardial perfusion imaging *J. Nucl. Med.* **47** 595–602
- Goorden M C, Rentmeester M C M and Beekman F J 2009 Theoretical analysis of full-ring multi-pinhole brain SPECT *Phys. Med. Biol.* **54** 6593–610
- Gruner S M, Tate M W and Eikenberry E F 2002 Charge-coupled device area x-ray detectors *Rev. Sci. Instrum.* **73** 2815–42
- He Z, Li W, Knoll G F, Wehe D K, Berry J and Stahle C M 1999 3-D position sensitive CdZnTe gamma-ray spectrometers *Nucl. Instrum. Methods A* **422** 173–8

- Heemskerk J W T 2010 Ultra-high resolution CCD-based gamma detection *PhD Thesis* Delft University of Technology, The Netherlands
- Heemskerk J W T, Korevaar M A N, Kreuger R, Ligtoet C M, Schotanus P and Beekman F J 2009 A micro-machined retro-reflector for improving light yield in ultra-high-resolution gamma cameras *Phys. Med. Biol.* **54** 3003–14
- Heemskerk J W T, Westra A H, Linotte P M, Ligtoet C M, Zbijewski W and Beekman F J 2007 Front-illuminated versus back-illuminated photon-counting CCD-based gamma camera: important consequences for spatial resolution and energy resolution *Phys. Med. Biol.* **52** N149–62
- Kataoka J, Saito T, Kuramoto Y, Ikagawa T, Yatsu Y, Kotoku J, Arimoto M, Kawai N, Ishikawa Y and Kawabata N 2005 Recent progress of avalanche photodiodes in high-resolution x-rays and γ -rays detection *Nucl. Instrum. Methods A* **541** 398–404
- Kim C L, Wang G C and Dolinsky S 2008 Multi-pixel photon counters for TOF PET detector and its challenges *IEEE Nucl. Sci. Symp. Conf. Record 2008* pp 3586–90
- King M A, Pretorius P H, Farncombe T and Beekman F J 2002 Introduction to the physics of molecular imaging with radioactive tracers in small animals *J. Cell. Biochem.* **39** (Suppl.) 221–30
- Korevaar M A N, Heemskerk J W T and Beekman F J 2009b A pinhole gamma camera with optical depth-of-interaction elimination *Phys. Med. Biol.* **54** N267–72
- Korevaar M A N, Heemskerk J W T, Goorden M C and Beekman F J 2009a Multi-scale algorithm for improved scintillation detection in a CCD based gamma camera *Phys. Med. Biol.* **54** 831–42
- Lees J E, Fraser G W, Keay A, Bassford D, Ott R and Ryder W 2003 The high resolution gamma imager (HRGI): a CCD based camera for medical imaging *Nucl. Instrum. Methods A* **513** 23–6
- Llosá G *et al* 2008 Evaluation of the first silicon photomultiplier matrices for a small animal PET scanner *IEEE Nucl. Sci. Symp. Conf. Record 2008* pp 3574–80
- Matteson J L *et al* 1997 CdZnTe arrays for astrophysics applications *Proc. SPIE* **3115** 160–75
- Meikle S R, Kench P, Kassiou M and Banati R B 2005 Small animal SPECT and its place in the matrix of molecular imaging technologies *Phys. Med. Biol.* **50** R45–61
- Menard L, Charon Y, Solal M, Laniece P, Mastrippolito R, Pinot L, Ploux L, Ricard M and Valentin L 1998 POCl: a compact high resolution gamma camera for intra-operative surgical use *IEEE Trans. Nucl. Sci.* **45** 1293–7
- Meng L J and Fu G 2008 Investigation of the intrinsic spatial resolution of an intensified EMCCD scintillation camera *IEEE Trans. Nucl. Sci.* **55** 2508–17
- Meng L J, Clinthorne N H, Skinner S, Hay R V and Gross M 2006 Design and feasibility study of a single photon emission microscope system for small animal I-125 imaging *IEEE Trans. Nucl. Sci.* **53** 1168–78
- Meng L J, Fu G, Roy E J, Suppe B and Chen C T 2009a An ultrahigh resolution SPECT system for I-125 mouse brain imaging studies *Nucl. Instrum. Methods A* **600** 498–505
- Meng L J, Tan J W, Spartiotis K and Schulman T 2009b Preliminary evaluation of a novel energy-resolved photon-counting gamma ray detector *Nucl. Instrum. Methods A* **604** 548–54
- Miller B W, Barber H B, Barrett H H, Shestakova I, Singh B and Nagarkar V V 2006 Single-photon spatial and energy resolution enhancement of a columnar CsI(Tl)/EMCCD gamma-camera using maximum-likelihood estimation *Proc. SPIE* **6142** 61421T
- Miller R G 1974 The jackknife—a review *Biometrika* **61** 1–15
- Miyata E, Miki M, Tawa N, Kamiyama D and Miyaguchi K 2004 Development of new X-ray imaging device sensitive to 0.1–100 keV *Nucl. Instrum. Methods A* **525** 122–5
- Nagarkar V V, Shestakova I, Gaysinskiy V, Tipnis S V, Singh B, Barber W, Hasegawa B and Entine G 2006 A CCD-based detector for SPECT *IEEE Trans. Nucl. Sci.* **53** (Part 1) 54–8
- Ostendorf B *et al* 2006 High-resolution multipinhole single-photon-emission computed tomography in experimental and human arthritis *Arthritis Rheum.* **54** 1096–104
- Peterson T E, Shokui S, Furenlid L R and Wilson D W 2009 Multi-pinhole SPECT imaging with silicon strip detectors *IEEE Trans. Nucl. Sci.* **56** 646–52
- Ponchut C, Zontone F and Graafsma H 2005 Experimental comparison of pixel detector arrays and CCD-based systems for x-ray area detection on synchrotron beamlines *IEEE Trans. Nucl. Sci.* **52** 1760–5
- Rentmeester M C M, Van Der Have F and Beekman F J 2007 Optimizing multi-pinhole SPECT geometries using an analytical model *Phys. Med. Biol.* **52** 2567–81
- Rogulski M M, Barber H B, Barrett H H, Shoemaker R L and Woolfenden J M 1993 Ultra-high resolution brain SPECT imaging—simulation results *IEEE Trans. Nucl. Sci.* **40** (Part 1) 1123–9
- Rowe R K, Aarsvold J N, Barrett H H, Chen J-C, Klein W P, Moore B C, Pang I W and White T A 1993 A stationary hemispherical SPECT imager for three-dimensional brain imaging *J. Nucl. Med.* **34** 474–80
- Russo P *et al* 2009 Imaging performance comparison between a LaBr₃:Ce scintillator based and a CdTe semiconductor based photon counting gamma camera *Med. Phys.* **36** 1298–317
- Schaart D R, Seifert S, Vinke R, Van Dam H T, Dendooven P, Löhner H and Beekman F J 2010 LaBr₃:Ce and SiPMs for time-of-flight PET: achieving 100 ps coincidence resolving time *Phys. Med. Biol.* **55** N179–89

- Schaart D R, Van Dam H T, Seifert S, Vinke R, Dendooven P, Löhner H and Beekman F J 2009 A novel, SiPM-array-based, monolithic scintillator detector for PET *Phys. Med. Biol.* **54** 3501–12
- Schramm N U, Ebel G, Engeland U, Schurrat T, Béhé M and Behr T M 2003 High-resolution SPECT using multipinhole collimation *IEEE Trans. Nucl. Sci.* **50** 315–20
- Seifert S, Schaart D R, van Dam H T, Huizenga J, Vinke R, Dendooven P, Löhner H and Beekman F J 2008 A high bandwidth preamplifier for SiPM-based TOF PET scintillation detectors *IEEE Nucl. Sci. Symp. Conf. Record 2008* pp 1616–9
- Shokouhi S, Metzler S D, Wilson D W and Peterson T E 2009 Multi-pinhole collimator design for small-object imaging with SiliSPECT: a high-resolution SPECT *Phys. Med. Biol.* **54** 207–25
- Soesbe T C, Lewis M A, Richer E, Slavine N V and Antich P P 2007 Development and evaluation of an EMCCD-based gamma camera for preclinical SPECT imaging *IEEE Trans. Nucl. Sci.* **54** 1516–24
- Van Dam H T, Seifert S, Vinke R, Dendooven P, Löhner H, Beekman F J and Schaart D R 2010 A comprehensive model of the response of silicon photomultipliers *IEEE Trans. Nucl. Sci.* **57** 2254–66
- Van Der Have F, Vastenhouw B, Ramakers R, Branderhorst W, Krah J O, Ji C, Staelens S G and Beekman F J 2009 U-SPECT-II: an ultra-high-resolution device for molecular small-animal imaging *J. Nucl. Med.* **50** 599–604
- Wagenaar D J, Chowdhury S, Engdahl J C and Burckhard D D 2003 Planar image quality comparison between a CdZnTe prototype and a standard NaI(Tl) gamma camera *Nucl. Instrum. Methods A* **505** 586–9
- Westra A H, Heemskerk J W T, Korevaar M A N, Theuwissen A J P, Kreuger R, Ligtoet C M and Beekman F J 2009 On-chip pixel binning in photon-counting EMCCD-based gamma camera: a powerful tool for noise reduction *IEEE Trans. Nucl. Sci.* **56** 2559–65
- Yamamoto K, Yamamura K, Sato K, Kamakura S, Ota T, Suzuki H and Ohsuka S 2007 Development of multi-pixel photon counter (MPPC) *IEEE Nucl. Sci. Symp. Conf. Record 2007* pp 1511–5